Effect of Copper Content on Structural, Optical and Photovoltaic Characteristics of Manganese Oxide Thin Films Prepared by Pulsed-Laser Deposition Technique

Doaa T. Mohammed
Ghuson H. Mohammed

Department of Physics, College of Science, University of Baghdad, Baghdad, IRAQ

In the current study, a 1064nm Nd:YAG laser pulses with pulse duration of 9 ns, energy of 500 mJ and repetition rate of 6 Hz were used to produce Cu-doped MnO thin films. The doping concentration of the thin films was varied (0.03, 0.05, 0.07, and 0.09). The structural, morphological, and optical characteristics of the doped films were investigated. The results showed that the prepared structures are polycrystalline with cubic phase. The surface morphology of the prepared samples suggests the formation of a sponge-like structure that covers all the surface. The grain size increases with increasing Cu concentration. The transmittance is inversely proportional to Cu concentration according to optical measurements. There is a noticeable blue shift in the UV-visible absorption spectra, which causes the optical bandgap to increase as the Cu concentration is increased. The effect of annealing at temperature of 200°C was studied. The Hall effect measurements demonstrate that all produced films exhibit p-type conductivity. Electrical properties of the $(MnO)_{1-x}Cu_x$/Si heterojunction solar cells were studied and the efficiency was found to decrease as the Cu concentration is increased.

Keywords: Manganese oxide; Solar cells; Thin Films; Photovoltaic properties
Received: 03 December 2023; **Revised:** 17 January; **Accepted:** 23 January 2024

1. Introduction

In recent years, manganese oxides have been given a great interest and promising transition metal oxide due to their various proprieties which that make them gaining interest in technological applications, such as sensor applications, magnetic storage media, solar cell applications, etc. [1,2]. Manganese oxide (MnO) is an n-type semiconductor with direct band gap around 2.33 eV and high optical absorption in the visible region that make it good candidate for optoelectronic applications, gas sensors, optical memory, and solar energy converters [3,4]. Many research works have been published on the synthesis and characterization of MnO thin films doped with aluminum (Al), silver (Ag), cobalt (Co), chromium (Cr), etc. [5-8]. In addition to these metals, copper (Cu) has good specifications as dopant material due to its low cost, good electrical conductivity, non-toxicity and environmentally friendly nature [9]. Doping MnO with copper may reasonably enhance electrochemical behavior [10]. The promising results from Cu-doped MnO nanoparticles have motivated further studies particularly focusing on the effect of doping level on the performance of MnO solar cells [11]. This is attributed to the advantages of transition metal oxide (MnO), mainly good chemical stability, transparency, low toxicity, low cost, functional biocompatibility, excellent adsorption capacity, catalytic properties, widespread availability and wide range of oxidation numbers [12,13]. Due to its low cationic doping has been proved to be effective to improve the conductivity, copper cations are found to improve electrochemical performance far better compared to other cations [9]. MnO thin films are widely used in bio-sensors [14], gas sensors [15], catalysis, electromagnetic wave-absorbing layers, high-performance electrochemical electrodes and energy storage devices [16]. The electrical characteristics of MnO compound was studied both theoretically and experimentally [17]. Due to its high potential capacity (755 mAh/g) and low electromotive force (e.m.f.) level (1.032V against Li/Li^+), MnO is used in catalysis, battery technologies, electrodes, energy storage, ion exchange, biomedical imaging, and drug delivery due to its unique properties [18,19].

Numerous attempts to prepare MnO nanostructures using chemical methods were presented, including the hydrothermal approach, wet chemical method, and spray pyrolysis technique [20]. Considerable research effort has been devoted to the preparation and characterization of MnO nanostructures doped with various metals employing spray pyrolysis, atomic layer deposition, and pulsed-laser deposition (PLD) [21,22]. Copper, on the other hand, is a diligent dopant of MnO due to its inexpensiveness, excellent electrical conductivity, nontoxicity, and eco-friendliness.

Here, we investigate the effects of annealing temperature on the electrical, optical, and structural characteristics of MnO thin films doped with variable

amounts of copper nanoparticles using the PLD technique for solar cell applications.

2. Experimental Part

The MnO with 99.99% purity was blended with different concentrations of Cu nanoparticles (0.03, 0.05, 0.07, and 0.09). The powder was blended for five minutes in a gate mortar then it was compressed using a hydraulic press at a pressure of 5 tons for a duration of 10 minutes. Pellets measuring 0.2 cm in thickness and 1 cm in diameter were produced. The pellets underwent an hour of sintering at 400°C before being cooled to room temperature.

The pellets were utilized to prepare thin films of $(MnO)_{1-x}Cu_x$ on 2.5x7.5cm glass substrates cleaned for 15 minutes with ultrasonic waves and distilled water. These films were deposited by PLD using a Nd:YAG laser with 500 mJ energy and 300 laser shots at a frequency of 6 Hz and 45° inclination with respect to the target surface. The deposition chamber was evacuated down to 10^{-2} mbar and the target was placed 1.5 cm away from the substrate. The interference method was used to estimate the layer thickness of about 200±5 nm. Finally, thin films were thermally annealed at 200°C for one hour using an electric oven.

A Philips PW1730 X-ray diffractometer (CuKα, λ=0.154nm) was utilized to study the structural properties of $(MnO)_{1-x}Cu_x$ thin films in the scanning range of 10°-80°. Atomic force microscopy (AFM) was used to examine the topography of the prepared films. A Metertech SP8001 UV-Vis-NIR spectrophotometer was used to study the optical properties of thin films in the wavelength range of 190-1100 nm.

3. Results and Discussion

Figure (1) shows the x-ray diffraction (XRD) patterns of undoped and Cu-doped MnO samples with different Cu contents. Samples with low Cu content indicates few Cu impurities in MnO lattice. The XRD patterns confirm that all films display polycrystalline cubic structure with no further impurity of Mn metal and oxides. This result agrees with that of Xia et al. [20-23]. The XRD patterns also show that the undoped and Cu-doped MnO samples have two high peaks and three lower ones, those are ascribed to polycrystalline structure. They are mostly oriented along (111), (200) and (220), (311) and (222) planes which corresponding to diffraction angles of 35.31°, 40.78°, 59.15°, 70.79° and 73.75°, respectively, according to ICCD cards 96-900-6666. The diffraction peak identified at (200) exhibits a preference orientation that has the lowest surface energy in face-centered cubic (FCC) structures, which agrees with literature [24]. Also, the incorporation of Cu into the MnO lattice shows a vital aspect in the film structure. There are some shift in the peaks resulting from substituting Cu–ions instead of Mn-ions which is larger than Mn due to the variation of distance between the internal planes. Additionally, due to the fact that the atomic radii of Cu particles are larger than those of MnO leads to Cu being substituted interstitially in the MnO lattice. This leads to increase of defect states in the MnO lattice caused by the increase of Cu doping ratio.

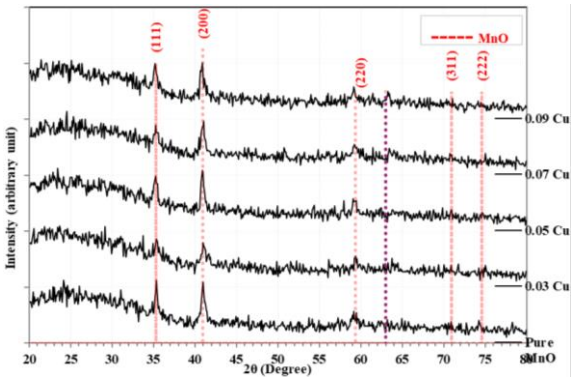

Fig. (1) XRD patterns of MnO thin films doped with Cu nanoparticles at various concentrations at annealing temperature of 200°C

The Debye-Scherrer's formula was used to determine the crystallite size [25,26]:

$$C_s = \frac{0.9\lambda}{\beta \cos\theta} \quad (1)$$

where λ represents the wavelength of the x-ray photons, β represents the full-width at half maximum (FWHM) after the base correction has been made, and θ represents the most significant angle of diffraction at the greatest peak, and the shape factor number is taken to be 0.9. The intermolecular planar space (d_{hkl}) can be found using Bragg's formula as [27]:

$$n\lambda = 2d_{hkl} \sin\theta \quad (2)$$

The average strain (ε) of nanoparticles is calculated using the Stokes-Wilson equation [28]:

$$\varepsilon = \frac{\beta_{hkl}}{4\ tan\theta} \quad (3)$$

To find the dislocation density (δ) that can be defined by the length of the dislocation lines to the crystallite size, the following relation is used [28]:

$$\delta = \frac{1}{C.S^2} \quad (4)$$

Table (1) shows the influence of Cu doping on particle size of MnO films on the most preferred (211) plane. As the percentage amount of Cu in MnO thin films grows from 0 to 9%, the crystallite size increases from 15 to 17 nm. Consequently, copper exhibits the characteristics of an interstitial dopant in the MnO lattice. This was claimed before as the increase in Cu doping level causes an increase in defect states in the lattice MnO.

The effects of different Cu concentrations (0.03, 0.05, 0.07, and 0.09 wt.) on the optical characteristics of MnO films annealed at 200°C were studied, including transmittance, absorption coefficient, and energy bandgap in the spectral range of 400-1100nm. The optical transmission spectra of both undoped and Cu-doped MnO films are displayed in Fig. (2). In the visible-NIR range (400-1100nm), film transmittance

steadily decreases with increasing Cu concentration, which may be attributed to increasing light absorption by the electrons excited from valence band (VB) to conduction band (CB). It is also observed that thin films exhibited a red shift in the absorption spectrum, which is mainly attributed to the change in crystalline structure.

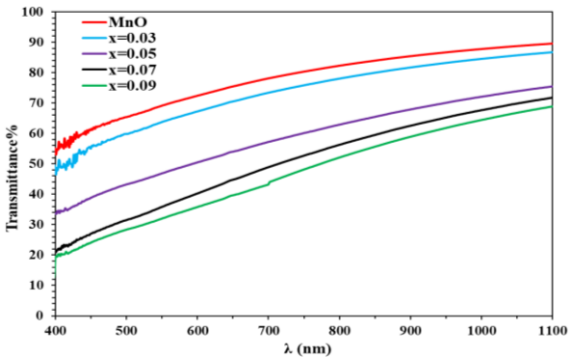

Fig. (2) Transmission spectra of MnO thin films doped with Cu nanoparticles at various concentrations at annealing temperature of 200°C

A negative and a positive correction are brought about the conduction and valence band edges as a result of the "*sp-d*" exchange interaction that occurs between the band electrons and the localized *d* electrons of the Mn^{4+} ions and the Cu^{+} ions. The *s-p* and *p-d* exchange interactions are responsible for the decrease in the energy band gap (E_g) [29].

The absorption coefficient can be calculated using the following relation [30]:

$$\alpha = 2.303\frac{A}{t} \quad (5)$$

where *A* denotes absorbance and *t* denotes sample thickness

Figure (3) depicts the variation of the absorption coefficient (α) of Cu-doped MnO thin films as a function of wavelength. The plots show that the absorption coefficients are high ($\alpha > 10^4$ cm^{-1}), which suggests that there is likely to be a straight electronic transition in these films. Also, it is clear that the absorption coefficient (α) of Cu-doped MnO films is high at short wavelengths and low at long wavelengths. Increasing Cu content in MnO lattice leads to an increase in the value of α, just like the behavior of transmittance with Cu content. The values of absorption coefficient (α) are tabulated in table (2).

The optical energy gap (E_g) can be estimated using the following relationship [31]:

$$\alpha h\nu = B\left(h\nu - E_g\right)^r \quad (6)$$

where *B* is a constant, which is independent of optical band gap energy while inversely related to the degree of amorphousness, and *r* is a constant that determines the type of optical transition and its value is equal to 2 for the direct allowed transition of the material, $h\nu$ is the photon energy

The Tauc formula states that the $(\alpha h\nu)^2$ diagram should be created in accordance with ($h\nu$). Figure (4) shows the optical band gap of Cu-doped MnO thin films at different Cu concentrations. This figure shows MnO has band gap of 3 eV, which decreases to 2.20 eV with Cu.

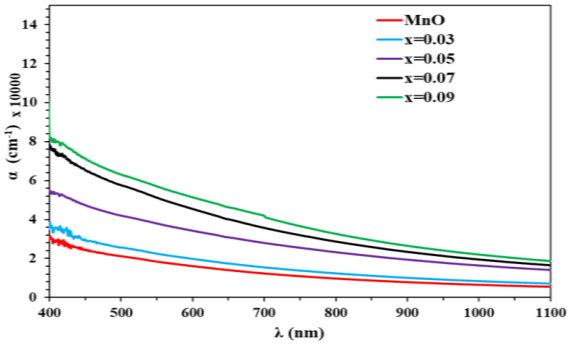

Fig. (3) Absorption coefficient of MnO thin films doped with Cu nanoparticles at various concentrations at annealing temperature of 200°C

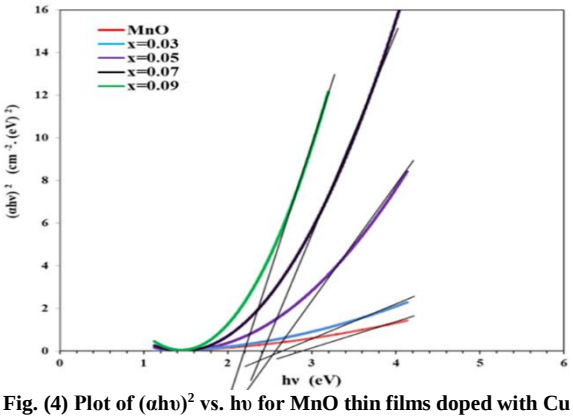

Fig. (4) Plot of $(\alpha h\upsilon)^2$ vs. hυ for MnO thin films doped with Cu nanoparticles at various concentrations at annealing temperature of 200°C

Because Cu sheets have functional groups on their surface, the inclusion of Cu enhances the ability of MnO thin films to absorb visible light. As some unpaired electrons were linked to the free electrons on the MnO surface, the value of band gap drops and the edge of valence band shifts upward. Values of energy bad gap are listed in table (2).

All previous results were considered to fabricate a solar cell. The photocurrent measured under irradiation with 100 mW/cm^2 visible light is shown in Fig. (5), which demonstrates the characteristics of current density (J) versus voltage (V) for undoped and Cu-doped MnO films. The results indicate that Cu-doped MnO thin films on Si substrates are useful as a solar cell. Figures (6-9) and table (3) show the J-V characteristics and the J-V parameters, mainly, open-circuit voltage (V_{oc}), short-circuit (I_{sc}), maximum voltage (V_m), maximum current (I_m), fill factor (F.F.), and efficiency (η). Generally speaking, it is seen that the I_{sc} increases as the Cu content is increased. It is noteworthy that, in comparison to the undoped MnO, the Cu-doped MnO solar cell fabricated at annealing temperature of 200°C exhibits a notable improvement in performance.

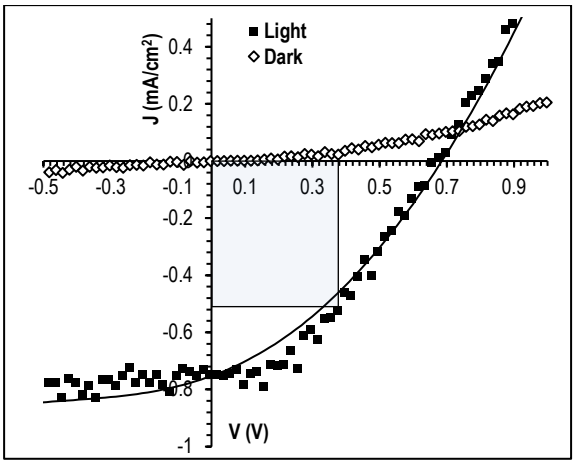

Fig. (5) J-V characteristics for MnO/p-Si annealed at 200°C when illuminated by 100 mW/cm^2 of white light

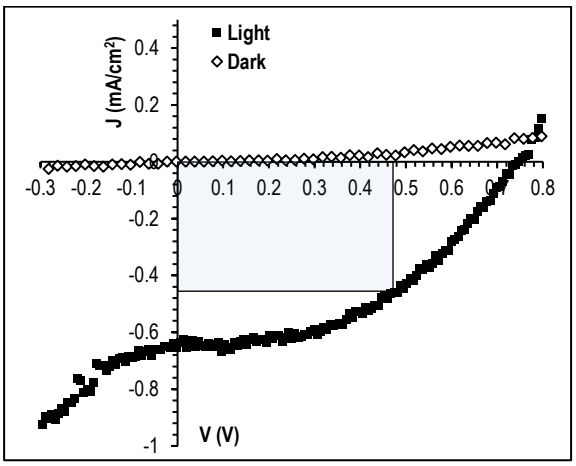

Fig. (6) J-V characteristics for $(MnO)_{1-x}Cu_x$/p-Si with Cu content of 0.03 at 200°C when illuminated by 100 mW/cm^2 white light

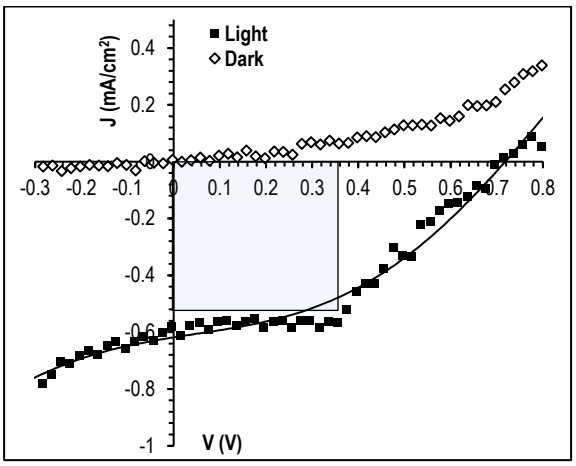

Fig. (7) J-V characteristics for $(MnO)_{1-x}Cu_x$/n-Si with Cu content of 0.05 at 200°C when illuminated by 100 mW/cm^2 white light

For undoped and Cu-doped MnO thin films, the power conversion efficiencies were found to be 17% and 23%, respectively. When the Cu content is increased, an increase in the fill factor and efficiency values is observed. This result agrees with that of Peng et al. [32]. Defects in thin films, such as states or vacancies, decrease with increasing Cu content; therefore, the photocurrent increases is proportional to the increase of Cu content.

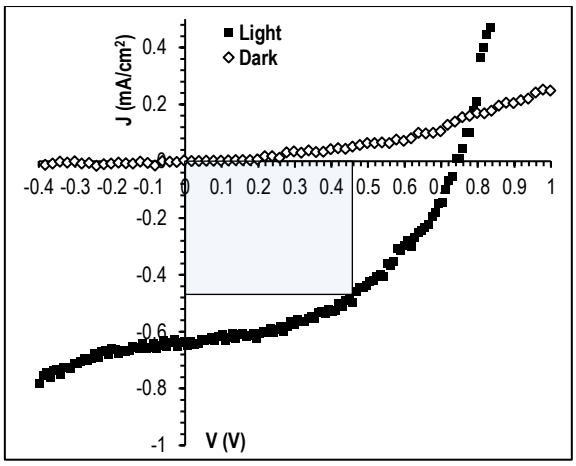

Fig. (8) J-V characteristics for $(MnO)_{1-x}Cu_x$/n-Si with Cu content of 0.07 at 200°C when illuminated by 100 mW/cm^2 white light

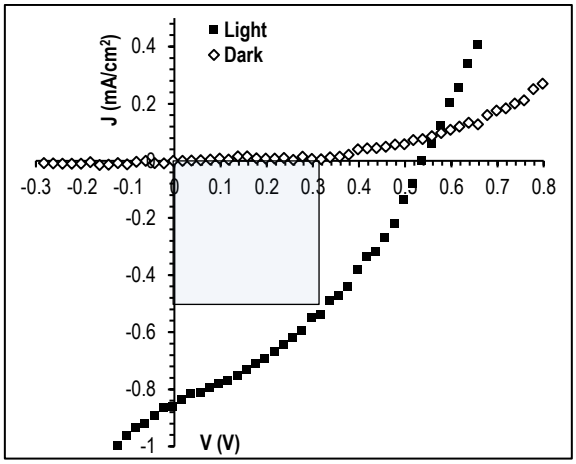

Fig. (9) J-V characteristics under illumination by 100mW/cm2 white light for $(MnO)_{1-x}Cu_x$/n-Si with Cu content of 0.09 annealed at 200°C

4. Conclusion

In concluding remarks, the valence state of Cu^{+2} plays a great role in the structural and optical properties of Cu-doped MnO thin films prepared by PLD technique. These films were polycrystalline with cubic structure and a preferential orientation along the (200) plane. The decrease in crystallinity of the MnO films with increasing doping level is attributed to precipitation of the dopants on the grain boundaries, which would hinder the recrystallization of MnO. This resulted in a redshift in the optical absorption edge as well as a decrease in the band gap from 2.90eV for the undoped MnO films to 2.20eV with Cu dopant. For undoped and Cu-doped MnO films, the power conversion efficiency was increased from 17% to 23%, respectively.

References

[1] A. Mabrouki et al., "Experimental study and DFT calculation of the oxygen deficiency effects on structural, magnetic and optical properties of $La_{0.8}Y_{0.2}MnO_{3-\delta}$ (δ= 0, 0.1 and 0.2) compounds", *J. Alloys Compd.*, 860 (2021) 157922.

[2] A. Mabrouki et al., "Oxygen deficiency effect on the magnetocaloric and critical phenomena for $La_{0.8}Y_{0.2}MnO_{3-\Delta}$ (Δ= 0, 0.1 and 0.2) compounds: significant enhancement of relative cooling power", *J. Mater. Sci. Mater. Electron.*, 31(24) (2020) 22749-22767.

[3] S. Massidda et al., "Band-structure picture for MnO reexplored: a model GW calculation", *Phys. Rev. Lett.*, 74(12) (1995) 2323.

[4] A.R. Armstrong and P.G. Bruce, "Synthesis of layered $LiMnO_2$ as an electrode for rechargeable lithium batteries", *Nature*, 381(6582) (1996) 499-500.

[5] M.S. Sheikh et al., "Narrow band gap and optical anisotropy in double perovskite oxide Sm_2NiMnO_6: a new promising solar cell absorber", *Sol. Energy Mater. Sol. Cells*, 193 (2019) 206-213.

[6] M. Zahan and J. Podder, "Structural, optical and electrical properties of Cu:MnO_2 nanostructured thin films for glucose sensitivity measurements", *SN Appl. Sci.*, 2 (2020) 1-12.

[7] K.A. Aadim and A.S. Jasim, "Silver nanoparticles synthesized by Nd:YAG laser ablation technique: characterization and antibacterial activity", *Karbala Int. J. Mod. Sci.*, 8(1) (2022) 71-82.

[8] F.J. Kadhim et al., "Photocatalytic activity of Ag-doped TiO_2 nanostructures synthesized by DC reactive magnetron co-sputtering technique", *Opt. Quantum Electron.*, 52(4) (2020) 188.

[9] D. An et al., "Synthesis of copper-doped MnO2 electrode materials by one-step hydrothermal method for high performance", *Acta Chim. Slov.*, 66(3) (2019) 584-591.

[10] S. Datta et al., "Enhanced performance of dye-sensitized solar cell with thermally stable natural dye-assisted TiO_2/MnO_2 bilayer-assembled photoanode", *Mater. Renew. Sustain. Energy*, 9 (2020) 1-11.

[11] B. Aljafari et al., "Copper doped manganese dioxide as counter electrode for dye-sensitized solar cells", *Arab. J. Chem.*, 15(9) (2022) 104068.

[12] X. Su et al., "Controllable hydrothermal synthesis of Cu-doped δ-MnO_2 films with different morphologies for energy storage and conversion using supercapacitors", *Appl. Energy*, 134 (2014) 439-445.

[13] E.C. Njagi et al., "Total oxidation of CO at ambient temperature using copper manganese oxide catalysts prepared by a redox method", *Appl. Catal. B Environ.*, 99(1/2) (2010) 103-110.

[14] Y. Liu et al., "Porous Ag-doped MnO_2 thin films for supercapacitor electrodes", *J. Porous Mater.*, 24 (2017) 1717-1723.

[15] Q. Tian et al., "Nanostructured $(Co, Mn)_3O_4$ for high capacitive supercapacitor applications", *Nanoscale Res. Lett.*, 12 (2017) 1-7.

[16] A.M. El Sayed and M. Shaban, "Structural, optical and photocatalytic properties of Fe and (Co, Fe) co-doped copper oxide spin coated films", *Spectrochim. Acta Part A Mol. Biomol. Spectrosc.*, 149 (2015) 638-646.

[17] M. Anilkumar and V. Ravi, "Synthesis of nanocrystalline Mn_3O_4 at 100°C", *Mater. Res. Bull.*, 40(4) (2005) 605-609.

[18] A. Kumar, M. Kumar, and R.P. Singh, "Study on electronic, magnetic, optical and thermoelectric properties of manganese oxide (MnO): DFT based spin polarized calculations", *Optik*, 241 (2021) 167064.

[19] O.A. Hammadi, "New technique to synthesize silicon nitride nanopowder by discharge-assisted reaction of silane and ammonia", *Mater. Res. Exp.*, 8 (2021) 085013.

[20] B.K. Pandey, A.K. Shahi and R. Gopal, "Synthesis, optical properties and growth mechanism of MnO nanostructures", *Appl. Surf. Sci.*, 283 (2013) 430-437.

[21] H. Jamil et al., "Structural and optical properties of manganese oxide thin films deposited by pulsed laser deposition at different substrate temperatures", *Laser Phys.*, 27(9) (2017) 96101.

[22] R.A. Ismail et al., "Full characterization at 904 nm of large area Si p-n junction photodetectors produced by LID technique", *The Euro. Phys. J. Appl. Phys.*, 38(3) (2007) 197-201.

[23] H. Xia et al., "Manganese oxide thin films prepared by pulsed laser deposition for thin film microbatteries", *Mater. Chem. Phys.*, 143(2) (2014) 720-727.

[24] D.T. Mohammed and G.H. Mohammed, "Investigation of Structural, Optical and Electrical Properties of MnO Doped with Cu Thin Films Prepared by PLD Technique for Solar Cell Applications", *East Eur. J. Phys.*, 3 (2023) 391-399.

[25] A.A. Almaula, Ç.Y. Ataol and G.H. Mohammed, "Structural and Optical Properties Study of SnS:Ag Doped Cu Thin Films Prepared by PLD Technique for Solar Cell Application", *J. Pharm. Negat. Resul.*, 13(4) (2022) 936-944.

[26] H.P. de Macedo et al., "Characterization of $ZnAl_2O_4$ spinel obtained by hydrothermal and microwave assisted combustion method: a comparative study", *Mater. Res.*, 20 (2017) 29-33.

[27] G.H. Mohammed et al., "Structural and Optical properties of CdO doped TiO_2 thin films prepared by Pulsed Laser Deposition", *Eng.*

Technol. J., 33(5B) (2015).
[28] B.D. Cullity and S.R. Stock, **"Elements of X-ray Diffraction"**, 3rd ed., Prentice Hall (NY, 2001), pp. 174-177.
[29] C.S. Barrett and M. TB, "Structure of metals. Crystallographic methods, principles and data", (1980).
[30] C. Kittel and P. McEuen, **"Introduction to Solid State Physics"**, John Wiley & Sons (2018).
[31] G.K. Williamson and R.E. Smallman, "III. Dislocation densities in some annealed and cold-worked metals from measurements on the X-ray debye-scherrer spectrum", *Philos. Mag.*, 1(1) (1956) 34-46.
[32] M.A. Abood and B.A. Hasan, "A Comparison Study the Effect of Doping by Ga_2O_3 and CeO_2 On the Structural and Optical Properties of SnO_2 Thin Films", *Iraqi J. Sci.*, (2023) 1675-1690.
[33] J. Millman and A. Grabel, **"Microelectronics"**, McGraw-Hill (NY, 1987).
[34] S.R. Elliott, **"Physics of Amorphous Materials"**, Longman Group, Ltd. (London, 1984).
[35] A. Peng et al., "MoC/MnO composite materials as high efficient and stable counter electrode catalysts for dye-sensitized solar cells", *J. Mater. Sci. Mater. Electron.*, 31 (2020) 1976-1985.

Table (1) The XRD parameters of MnO thin films doped with different concentrations of Cu NPs annealed at 200°C

Sample	2θ (Deg.)	FWHM (Deg.)	d_{hkl} Std.(Å)	C.S. (nm)	(hkl)	Phase
MnO	40.94	0.5637	2.2027	15.0	(200)	MnO
MnO:Cu (0.03)	40.98	0.4832	2.2006	17.6	(200)	MnO
MnO:Cu (0.05)	35.22	0.5235	2.5460	15.9	(111)	MnO
MnO:Cu (0.07)	41.06	0.4832	2.1965	17.6	(200)	MnO
MnO:Cu (0.09)	41.11	0.4833	2.1940	17.6	(200)	MnO

Table (2) The transmittance, absorption coefficient, and optical energy gap of MnO thin films doped with different concentrations of Cu NPs annealed at 200°C

Sample	Transmittance (%)	Absorption Coefficient α (cm^{-1})	Energy Band Gap E_g (eV)
MnO	65.43	2.1212	2.90
MnO:Cu (0.03)	45.21	3.196	2.70
MnO:Cu (0.05)	59.88	3.564	2.60
MnO:Cu (0.07)	31.54	5.769	2.40
MnO:Cu (0.09)	28.32	6.308	2.20

Table (3) Photovoltaic parameters of MnO thin films doped with different concentrations of Cu NPs annealed at 200°C to form $(MnO)_{1-x}Cu_x$/p- and n-Si heterojunctions irradiated by 100 mW/cm^2 white light

Sample	I_{sc} (mA)	I_m (mA)	V_{oc} (V)	V_m (V)	F.F.	Efficiency η (%)	ideality factor (β)
MnO	0.54	0.53	0.86	0.32	0.37	0.17	2.41
MnO:Cu (0.03)	0.74	0.53	0.65	0.36	0.40	0.19	2.16
MnO:Cu (0.05)	0.60	0.56	0.70	0.36	0.48	0.20	1.56
MnO:Cu (0.07)	0.74	0.48	0.65	0.46	0.46	0.22	1.39
MnO:Cu (0.09)	0.64	0.50	0.73	0.46	0.49	0.23	1.07

